Remote Sensing of Environment 113 (2009) 563–570

Contents lists available at ScienceDirect

Remote Sensing of Environment

journal homepage: www.elsevier.com/locate/rse

Comparison of Envisat radar and airborne laser altimeter measurements over Arctic sea ice

Laurence N. Connor [a,*], Seymour W. Laxon [b], Andrew L. Ridout [b], William B. Krabill [c], David C. McAdoo [a]

[a] NOAA, E/RA31, SSMC1, Laboratory for Satellite Altimetry, 1335 East–West Highway, Silver Spring, Maryland 20910-3226, USA
[b] Centre for Polar Observation and Modelling, University College London, Gower Street, London, WC1E 6BT, UK
[c] NASA Goddard Space Flight Center, Cryospheric Sciences Branch, Code 614.1, Wallops Island, Virginia 23337, USA

ARTICLE INFO

Article history:
Received 24 April 2008
Received in revised form 22 September 2008
Accepted 22 October 2008

Keywords:
Satellite altimetry
Radar altimeter
Laser altimetry
Sea ice thickness
Snow depth

ABSTRACT

Sea ice thickness is a crucial, but very undersampled cryospheric parameter of fundamental importance for climate modeling. Advances in satellite altimetry have enabled the measurement of sea ice freeboard using satellite microwave altimeters. Unfortunately, validation of these new techniques has suffered from a lack of ground truth measurements. Therefore, an airborne campaign was carried out in March 2006 using laser altimetry and photo imagery to validate sea ice elevation measurements derived from the Envisat/RA-2 microwave altimeter.

We present a comparative analysis of Envisat/RA-2 sea ice elevation processing with collocated airborne measurements collected north of the Canadian Archipelago. Consistent overall relationships between block-averaged airborne laser and Envisat elevations are found, over both leads and floes, along the full 1300 km aircraft track. The fine resolution of the airborne laser altimeter data is exploited to evaluate elevation variability within the RA-2 ground footprint. Our analysis shows good agreement between RA-2 derived sea ice elevations and those measured by airborne laser altimetry, particularly over refrozen leads where the overall mean difference is about 1 cm. Notwithstanding this small 1 cm mean difference, we identify a larger elevation uncertainty (of order 10 cm) associated with the uncertain location of dominant radar targets within the particular RA-2 footprint. Sources of measurement uncertainty or ambiguity are identified, and include snow accumulation, tracking noise, and the limited coverage of airborne measurements.

Published by Elsevier Inc.

1. Introduction

The areal extent of Arctic sea ice, and its generally negative trend of about 10% depletion per decade since 1979, have been well monitored by passive microwave satellites (e.g., Comiso, 2002). However, accurate knowledge of sea ice thickness and its spatial and temporal variability have been more difficult to acquire. Submarine and other in-situ observations of ice thickness (Rothrock et al., 1999), while they indicate a thinning, are sparse and infrequent. But recently techniques have been demonstrated using satellite altimetry, both radar (Laxon et al., 2003) and laser (Zwally et al., 2008), to monitor thickness. Thickness and extent of sea ice are important components of the ocean-atmosphere system in the Arctic, particularly in the ice-albedo feedback. Good estimates of ice thickness are critical for input into, and constraining of, global climate or coupled atmosphere-ocean models (e.g., McLaren et al., 2006) and for quantifying total sea ice mass and monitoring the global spatial and seasonal variations of this mass.

Sea ice thickness may be estimated using measurements of sea ice freeboard (i.e., ice elevation above local sea level) along with a characterization of the vertical density structure of sea ice. Both radar and laser altimeters have been used successfully to measure sea ice freeboard from satellites (Laxon et al., 2003; Kwok et al., 2004; Zwally et al., 2008). Laxon (1994), Laxon et al. (2003), have developed sea ice processing schemes whereby satellite microwave radar altimeter returns are retracked and optimized for sea ice, yielding estimates of sea ice freeboard and ice type characterization. This processing has been applied successfully to ERS-1 & 2 radar altimeters and the similar Envisat dual frequency RA-2 Radar Altimeter. Although these radar altimeters provide excellent coverage of all Arctic seas south of 81.5°N, the validation of such sea ice elevation measurements is hampered by the lack of surface truth data. To redress this lack of data, the Arctic Aircraft Altimeter (AAA) 2006 Campaign was carried out on March 27, 2006 to gather measurements of sea ice surface characteristics from multiple airborne instruments simultaneously with overpasses of the Envisat and ICESat satellites. This study focuses on Envisat radar measurements of sea ice elevations and does not attempt any examination of laser altimetry from ICESat. The Laser Radar Altimetry (LaRA) airborne field campaign of 2002 attempted to establish some validation of Envisat and ERS-2 altimetry over sea ice, but was limited

* Corresponding author.
E-mail address: Laurence.Connor@noaa.gov (L.N. Connor).

0034-4257/$ – see front matter. Published by Elsevier Inc.
doi:10.1016/j.rse.2008.10.015

to just a few useable ERS-2 and no Envisat data due to Envisat technical problems (Giles et al., 2007).A field campaign described by Leuschen et al. (2008) compared airborne laser and radar altimeter measurements, but no satellite altimetry, over Antarctic sea ice.

We present an analysis of airborne laser altimeter and photo imagery data collected during the AAA 2006 Campaign to explore the usefulness of these data in validating the sea ice elevations derived from RA-2 return waveforms and an associated processing scheme (Laxon et al., 2003; Laxon, 1994). A statistical comparison of RA-2 and spatially averaged ATM elevations is carried out to examine the general trends along the full Envisat leg of the AAA flight track (Fig. 1). More detailed examination is made of both the RA-2 sea ice elevations and ice type designations using the finer scale laser measurements and photo imagery. We find that Envisat radar satellite altimetry, with appropriate waveform processing, yields estimates of sea ice elevation that compare well with airborne laser altimetry measurements. The effects of uncertain snow depth are significant in laser-radar comparisons as laser altimeters will measure elevations of snow accumulated on sea ice while radar altimeters (operating in the Ku-band) will penetrate snow cover to measure elevations at the snow/ice interface (Beaven et al., 1995; Giles et al., 2007; Leuschen et al., 2008). Effects of snow penetration by the Envisat radar are carefully assessed in our study. In addition, we show how heterogeneities in the ice field, such as leads slightly offset from the satellite nadir, can in some instances corrupt Envisat elevation estimates and require careful interpretation.

2. Airborne data

Fig. 1 shows the March 27, 2006 flight path followed by a NASA P-3 aircraft during the AAA Campaign. Meteorological conditions observed during the flight, and confirmed by daily gridded NCEP data, were generally dry and cloud-free. The cloud-free conditions were verified by onboard photo imagery. The aircraft underflew the Envisat satellite, following the orbital ground track of Cycle 46, revolution 201. The AAA validation flight began at Point A (74.87° N, 143.42° W) at 19:28 UTC heading northeast. At ~80.5°N, the flight diverted north-west to underfly the ICESat satellite, then reversed its track to return to, and continue northeast along the Envisat track finishing at Point B (81.45° N, 92.26° W) near Nansen Sound at 23:50 UTC. The resulting flight path included over 1300 km of Envisat altimeter ground track and 300 km of ICESat/GLAS ground track. Validation of ICESat data is the subject of a separate investigation. The Envisat satellite was over Point B in Fig. 1 at 21:44 UTC and traversed to Point A at 21:47 UTC. The longest temporal separation between Envisat measurements and aircraft measurements was about 2 h 20 min at point B and the shortest separation of about 13 min occurred near 80.5°N. The ATM data swath was found to be offset southeast from the exact Envisat nadir ground track by about 200–500 m. The Envisat altimeter footprints are sufficiently large (nominally 2 to 10 km in diameter) that they still encompass the flight path.

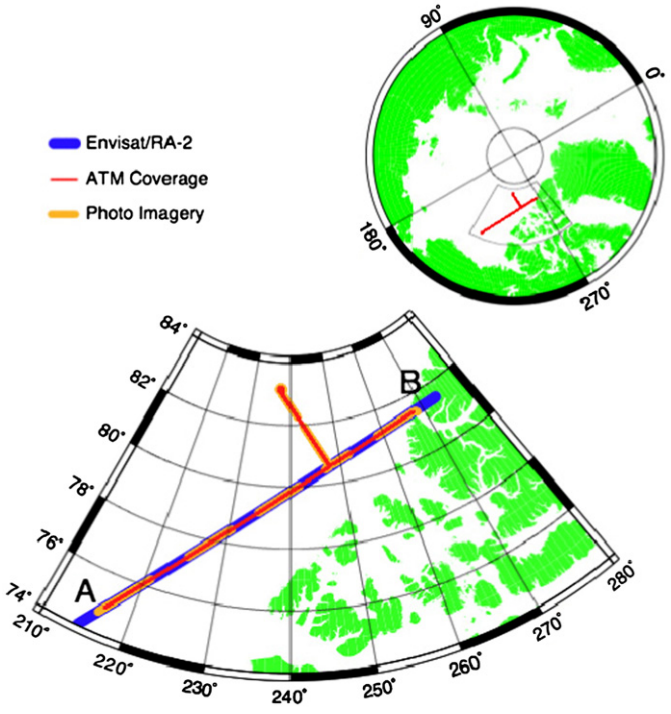

Fig. 1. Flight path followed by NASA P-3 aircraft during the Arctic Aircraft Campaign on March 27, 2006. Blue line is the under-flown Envisat track, red line indicates coverage of the ATM laser altimeter, and the yellow lines show the semi-continuous photo imagery coverage along the flight. (For interpretation of the references to colour in this figure legend, the reader is referred to the web version of this article.)

The aircraft was equipped with several instruments to monitor sea ice along the flight path. These included a laser altimeter, a microwave radar altimeter, a snow radar, and two bottom mounted digital cameras. Data collected from the Delay-Doppler Phase Monopulse (D2P) microwave radar altimeter (Leuschen & Raney, 2005) and the snow radar was unavailable for this study. Future analysis will include comparisons with measurements from the airborne microwave altimeter. This study focuses on measurements derived from the laser altimeter and the imagery provided by the cameras. The laser altimeter is NASA's Airborne Topographic Mapper (ATM). The ATM is a conical-scanning laser ranging system operated at a wavelength of 532 nm with a pulse repetition frequency of 5 kHz and a scan rate of 10 Hz with an off-nadir scan angle of 22° (Krabill et al., 2002). Aircraft location was determined with global positioning system (GPS) techniques, and aircraft heading, pitch, and roll were measured by inertial navigation systems. Typical flight parameters constrained the ATM observation geometry to an across-track scan swath of 400 m, the laser illuminating a 1 meter diameter footprint sampled approximately every 5 m along- and across-track near the center of the scan swath, the sampling becoming significantly finer (sub-meter) near the edges of the swath. The beam of the ATM generally backscatters sufficiently from a snow or ice surface to measure the time delay of a return signal and determine a total propagation distance. The rare presence of liquid water along the AAA flight path resulted in some measurement dropouts, probably due to the ATM beam being forward scattered by the extremely smooth surface. The travel time data were combined with GPS navigation measurements and aircraft orientation parameters to derive surface elevation measurements relative to the WGS84 reference ellipsoid, with a typical accuracy better than 10 cm (Krabill et al., 2002). Two Kodak DC4800 digital cameras were used to gather photographic imagery of the sea ice and snow surface along the flight path. Nominal surface coverage of a single image was 640 m (along-track)×420 m (across-track). Two cameras were necessary to assure image frame overlap along the flight path due to the refresh delay of the Kodak DC4800. Memory constraints on the cameras required the periodic downloading of images, resulting in the coverage gaps evident in Fig. 1.

3. Satellite altimeter data

Envisat is a European Space Agency (ESA) satellite which carries 10 earth observing instruments including the Radar Altimeter-2 (RA-2)—a pulse-limited nadir-looking, two-frequency (13.575 GHz in the Ku-Band is the primary frequency, 3.2 GHz in S-band is the secondary frequency) radar similar in function to its predecessors, ERS-1 and ERS-2, which also used Ku-band (13.8 GHz) altimeters. The Envisat RA-2 transmits 1800 pulses/s and averages 100 return pulses to generate 18 Hz waveforms. Such 18 Hz RA-2 waveform data collected during the AAA 2006 campaign were retracked and processed using

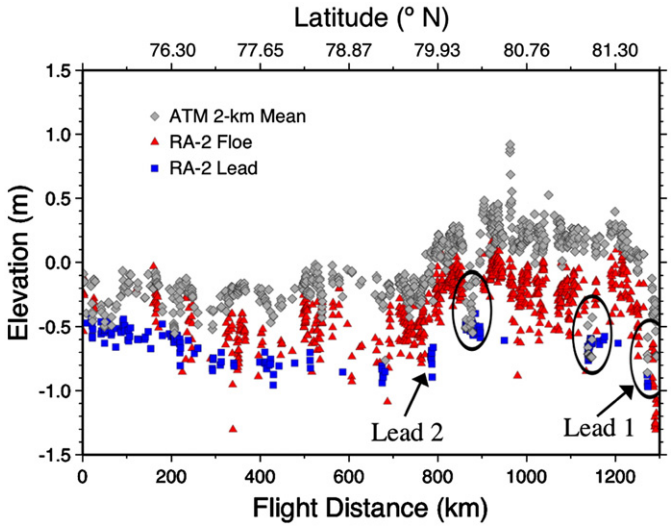

Fig. 2. ATM and RA-2 ice freeboard elevations along Envisat leg of AAA flight path. Red triangles and blue squares are RA-2 sea ice elevation estimates of floe and lead types, respectively. Grey diamonds are elevations derived from 2 km means of ATM measurements collocated with RA-2 points. All elevations are with respect to the TOPEX reference ellipsoid with a GRACE hybrid geoid removed. Encircled regions are areas of significant lead elevation agreement. Lead 1 and Lead 2 labels indicate the along-track location of specific examples also referred to in Fig. 4. (For interpretation of the references to colour in this figure legend, the reader is referred to the web version of this article.)

the techniques developed by Laxon (1994), Laxon et al. (2003) to yield sea ice elevations at an 18 Hz sample rate, which corresponds to a sample every 370 m along the satellite ground track. The corresponding surface footprint size is uncertain but has approximately a nominal 2–10 km diameter (see Chelton et al. 2001; Peacock & Laxon 2004, and discussion in Section 5 below). The Envisat results are derived from the RA-2 SGDR product (ESA, 2007). We apply the standard (SGDR) corrections for atmospheric propagation and tides, except for the dry tropospheric correction, which is derived from NCEP, the inverse barometer which is obtained from MOG2D (Carrère & Lyard, 2003), and the ionospheric correction which uses the GIM model (Iijima et al., 1999). During the sea ice processing, valid elevation measurements are assigned a descriptive category value of floe, lead, ocean, or unknown, based on the Pulse Peakiness (PP) criteria (Peacock & Laxon, 2004). Echoes with a PP less than 3 were classified as floes, and with a PP greater than 30 were classified as leads. The difference in thresholds as compared with Peacock and Laxon (2004) account for the wider recording window and more stable tracking of the RA-2 compared with the ERS altimeters. Echoes with PP values between 3 and 30, or with a leading edge width (Laxon, 1994) of greater than 4 samples, were classified as unknown. The criteria for unknown returns is designed primarily to remove echoes from mixed surfaces as commonly occurs when the radar off ranges to a bright lead away from the nadir point. The floe category refers to a discrete section of unbroken sea ice, bounded by leads (or refrozen leads) and usually consisting of relatively flat pieces of ice. While a lead is, strictly speaking, a linear, open-water feature, here the lead category usually refers to newly refrozen leads. The surfaces of refrozen leads are very flat and smooth, producing quasi-specular returns and an associated rapid drop in return power with increasing angle off-nadir (Peacock & Laxon, 2004; Laxon, 1994). Radar returns from ice floes are less specular, resulting in more diffuse returns and a slower drop in power. Elevations over floes are obtained using an OCOG retracker (Bamber, 1994) whilst those over leads are obtained by fitting a Gaussian function to the return echo. All valid RA-2 sea ice elevation estimates associated with the AAA flight track fall into the lead or floe category. The resulting data set includes 629 floe estimates and 157 lead estimates.

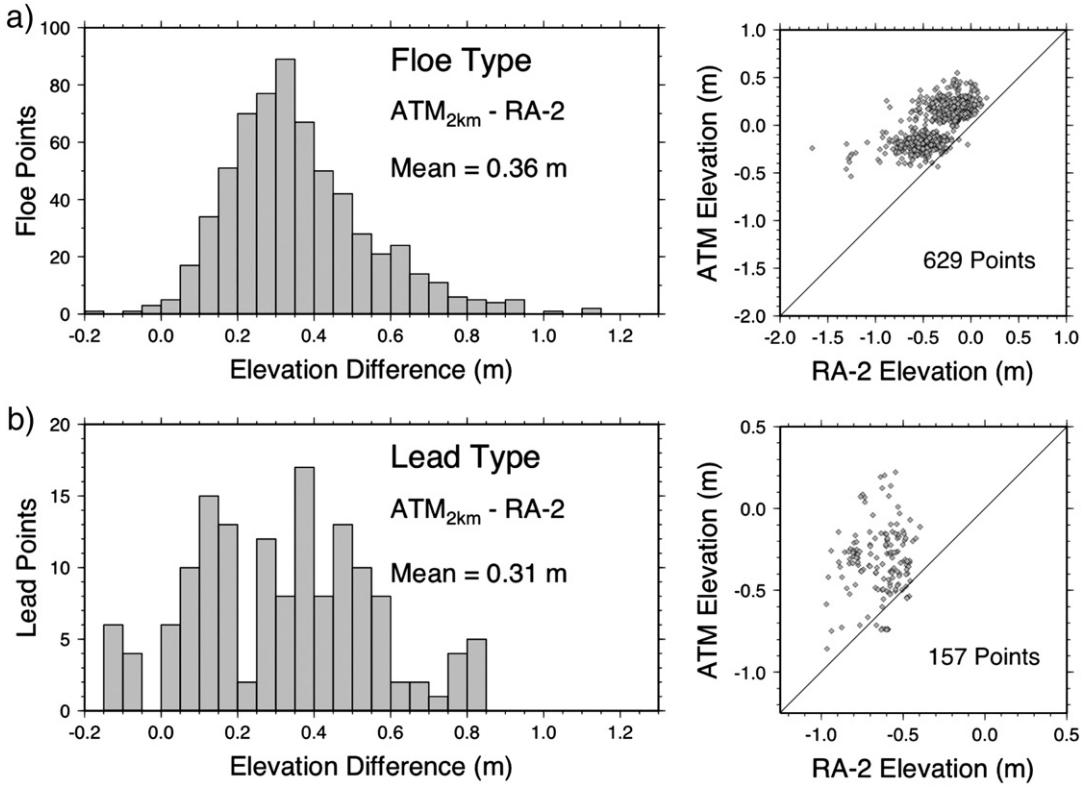

Fig. 3. (a) Top panel shows the histogram representation (left) of the differences of ATM 2 km mean elevations and RA-2 floe type elevations. A scatter plot of the ATM and RA-2 floe type elevations is shown to the right of the floe histogram. (b) Bottom panel shows the histogram of ATM 2 km mean and RA-2 lead type elevation differences with the corresponding scatter plot to the right.

4. Processing and observations

For comparison purposes, all elevation measurements from the ATM and the RA-2 were converted to the same physical reference frame, implementing the IERS or so-called TOPEX reference ellipsoid (Tapley et al., 1994) and removing a GRACE hybrid geoid model (McAdoo et al., 2005). Removing a geoid model effectively eliminates the dominant component of the elevation signal, leaving behind small-scale sea level anomaly features for more detailed examination. All ATM elevation measurements underwent an outlier removal procedure and were interpolated onto a 10 m × 10 m grid, aligned with the AAA flight track direction, using an inverse distance method with an 8 m radius.

Fig. 2 shows a comparison of RA-2 sea ice elevation estimates and collocated mean ATM elevations along the entire Envisat leg of the AAA flight track. The RA-2 elevations have been separated according to category, the red triangles indicating floe type and the blue squares indicating lead type. For each RA-2 elevation estimate, an ATM elevation mean was constructed by averaging all of the ATM elevation measurements within a 2 km along-track window centered on the geolocation coordinates of the RA-2 estimate. This was done in order to approximately match the spatial scales of the two types of elevation measurement. The RA-2 elevation estimates behave qualitatively according to the physical interpretation of their ice type category. The floe estimates show a clear trend of higher elevation over the lead estimates and have a larger variability, as might be expected with the rough topography associated with floe ice and the sea level elevations expected with leads and refrozen leads. A region of higher ice freeboard is seen above 80°N latitude along with a consistent increase of floe concentration.

Comparing RA-2 floe elevations with the collocated and averaged ATM elevations reveals a clear difference in the elevations measured by the two methods, with ATM being on order of 30–50 cm higher along the entire observation track. Previous comparisons (Giles et al. 2007; Leuschen & Raney, 2005; Leuschen et al., 2008) of coincident data from the laser and radar altimeters show that the laser elevations tend to be higher than the radar elevations over snow-covered sea ice and that the difference in elevations estimates between the two instruments may be an indicator of snow depth. In this study, we examine the hypothesis that the ATM measures snow or ice freeboard (the laser will not penetrate snow) while the RA-2 measures only ice freeboard. Ku-band microwaves will penetrate snow to the ice/snow interface. While some of the energy from the microwaves may penetrate the ice and produce volume scattering, most of the energy returned and measured by the RA-2 comes from surface scattering at the ice/snow (or ice/air) interface (Giles et al., 2007; Beavan et al., 1995). According to this hypothesis, our observed ATM-RA2 elevation differences (e.g., Fig. 2) should be, and are, physically consistent with the sea ice surface having an overall snow cover. The distribution of these differences may be seen in Fig. 3a through a histogram representation (left) of the elevation residuals (ATM-RA2) of floe points and a scatter plot (right) of the collocated ATM and RA-2 elevations. Here the elevation residuals range from 0 to 95 cm, peaking around 35 cm. The total mean residual value is 36 cm. While in situ measurements of snow depth on sea ice are very limited, these residual values are consistent with an Arctic snow depth climatology

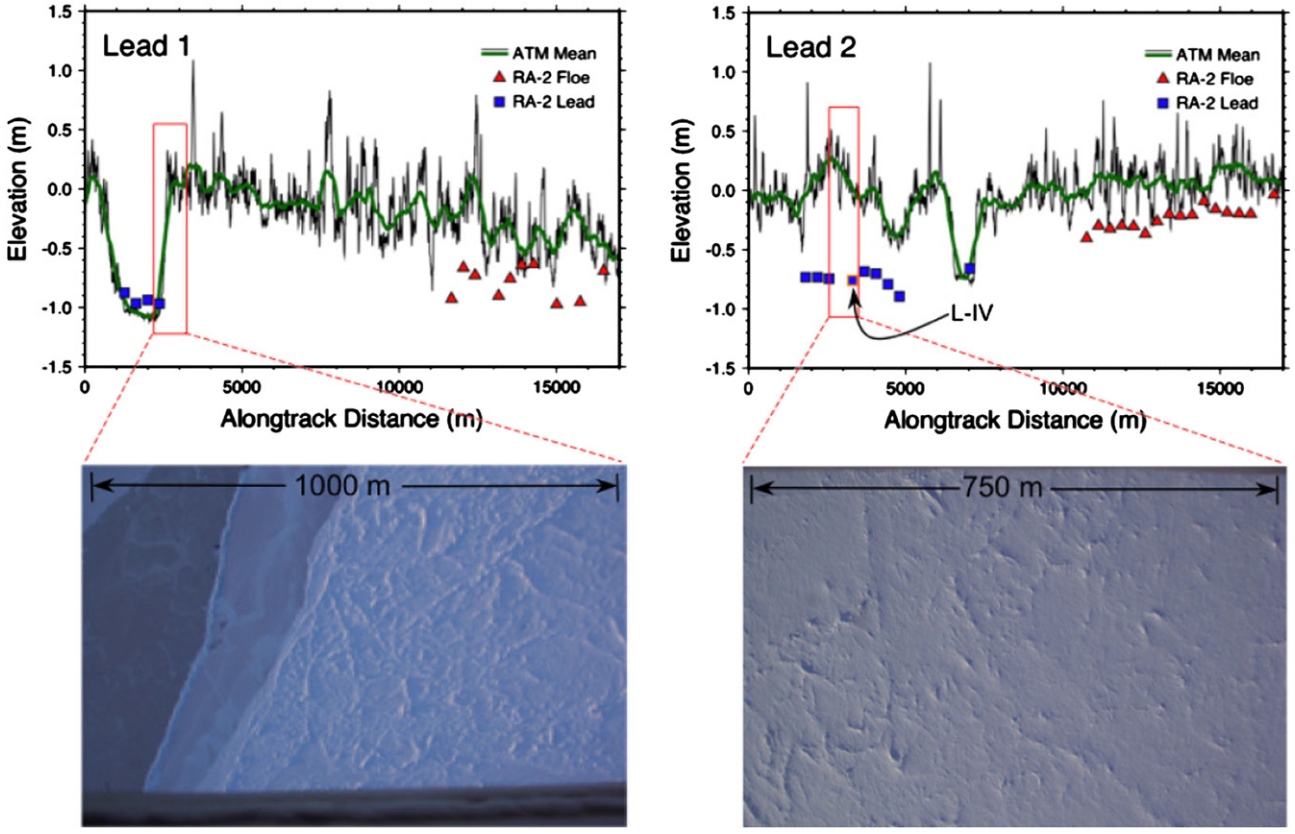

Fig. 4. Top panels show ATM elevation profiles (green and black lines) associated with Lead 1 and Lead 2 of Fig. 2. Red triangles and blue squares are RA-2 floe and lead elevations. All elevations are with respect to the TOPEX reference ellipsoid with a GRACE hybrid geoid removed. The downward slope of the elevation profile observed in the Lead 1 panel may result from shallow sea tides, dynamic topography, or geoid error. The images in the bottom panels show the photo imagery corresponding to the along-track regions enclosed in the red boxes of the profile plots. Lead 1 imagery reveals a clear lead to floe transition while Lead 2 imagery shows only a snow covered floe surface. The actual lead which gives rise to RA-2 Lead 2 elevations (e.g., L-IV bordered in orange) lies largely just out of view–and to one side–of the ATM and photo imagery swath (cf., MODIS scene in Fig. 5; also Fig. 6). (For interpretation of the references to colour in this figure legend, the reader is referred to the web version of this article.)

developed by Warren et al. (1999). The climatology is based on snow depth and density measurements at Soviet drifting stations on multiyear Arctic sea ice over 37 years (1954–1991) and shows a 34 cm snow depth over the region and season of the AAA campaign (Warren et al., 1999). An offset in the form of higher ATM elevation values is also evident in the scatter plot over the full range of RA-2 elevations, as expected with a significant snow cover.

The ATM 2 km mean elevations corresponding to the RA-2 lead estimates in Fig. 2 show an even greater elevation difference overall, with some exceptions occurring most notably near the circled regions. While it is expected that refrozen leads will generally have a lower freeboard elevation than floes, as borne out by the lower elevation trend in RA-2 lead points relative to floe points in Fig. 2, it initially seemed unusual that the ATM lead elevations in Fig. 2 did not better track lower elevations around the RA-2 designated leads. The residual histogram and scatter plot for these lead points (Fig. 3b) reveal a sporadic distribution of elevation differences spread over a wide range, from −20 cm to 85 cm, with peaks scattered between 10 cm and 50 cm and a total mean residual of 31 cm. This distribution seemed to imply significant snow accumulation over refrozen leads often exceeding that seen over floe ice, a geophysically unlikely event. Furthermore, the scatter plot representation revealed a somewhat vague relationship between the ATM and RA-2 lead elevation measurements with ATM elevations notably higher over the full range of RA-2 elevation values. This behavior will be discussed further in Section 5.

More detailed comparisons of ATM and RA-2 elevations are shown in the top panels of Fig. 4. The top-left panel of Fig. 4 shows an elevation profile produced from ATM measurements over a 17 km stretch of the AAA flight, located at Lead 1 in Fig. 2, and includes a transition from a region of refrozen lead to one of floe. The profiles depict an across-track mean calculated from the gridded ATM data (black line) and an along-track smoothed version of this mean (green line). RA-2 lead and floe elevations are represented by the blue squares and red triangles, respectively. We believe the downward slope observed in the elevation profile results from shallow sea tides, dynamic topography of the sea surface, or geoid error. The profile plot shows good agreement over a refrozen lead with elevation differences between the ATM means and the RA-2 estimates ranging from 0 to 15 cm. The floe measurements further down-track show an elevation difference between the ATM and RA-2 techniques of 30–100 cm, arguably associated with laser sensitivity to accumulated snow surfaces, though not precluding uncertainties from sampling differences and footprint size. The panel below this profile shows the photo imagery associated with the region of lead/floe transition encompassed by the red box in the profile. The refrozen lead is visibly free of any snow accumulation and abruptly changes to a region of snow covered floe ice as the flight path is traversed. The profile shown in the upper-right panel of Fig. 4 shows similar coverage over a region located at Lead 2 in Fig. 2. In contrast to the profile of Lead 1, the lead elevations measured by the RA-2 and the ATM in this profile show a significant separation of 40–100 cm. The photo imagery associated with the section of these lead points contained in the red box is shown in the lower-right panel of Fig. 4. This imagery shows a region of snow covered floe ice, a result qualitatively consistent with the elevation separation observed, but in apparent contradiction to the lead ice type assigned by the RA-2 sea ice processing.

5. Lead identification and analysis

The results presented in Figs. 3b and 4 at first seem difficult to understand, but are explicable upon careful examination. The 2 km 'window' used to form ATM elevation means and then compare with RA-2 is a simplistic attempt to put RA-2 and ATM measurements on comparable spatial scales. The 2 km window size was selected because it is a fair estimate of nominal footprint diameter of Ku-band altimeters, such as the RA-2, over open ocean with a flat sea state (Chelton et al., 2001). Indeed, it is known that where the radar reflective surface becomes inhomogeneous on the scale of the altimeter footprint, the precise point of origin of the detected echo can become ambiguous and may no longer be identified with the nadir location. In particular, the flat geometry of refrozen leads produces strong specular reflections at microwave wavelengths and the return radar signal from a region of mostly floe ice can easily be dominated by a signal associated with a small (as little as 1% of the surface), refrozen lead within the same radar footprint (Drinkwater, 1991; Fetterer et al., 1992; Peacock & Laxon, 2004). This problem may find its way into altimeter processing of sea ice waveforms when the altimeter passes from highly reflective refrozen lead surfaces to less reflective floe surfaces where the tracker may "snag" (Fetterer et al., 1992; Peacock & Laxon, 2004) on the more reflective lead surface as a preferential target, although it is off-nadir by several (1–10) km (see Chelton et al., 2001 for a discussion of footprint size).

The sensitivity of the RA-2 to the specular scattering of lead surfaces combined with the relatively narrow swath coverage of the ATM introduces several challenges in validating RA-2 sea ice elevations. These are demonstrated well in Fig. 5 which shows MODIS 250 m resolution visible imagery of the region encompassing the ATM and RA-2 measurements of the Lead 2 profile of Fig. 4 (right panel) near the time of the AAA flight (MODIS pass at 23:50 UTC). The MODIS imagery data was obtained from NASA's Level 1 and Atmosphere Archive and Distribution System (http://ladsweb.nascom.nasa.gov). The darker areas in the MODIS image reveal the leads and refrozen leads in the sea ice while the white areas indicate floe ice (Farrell, 2007; Peacock & Laxon, 2004). Green lines show the outside edges of the ATM swath along the AAA flight path, with blue squares

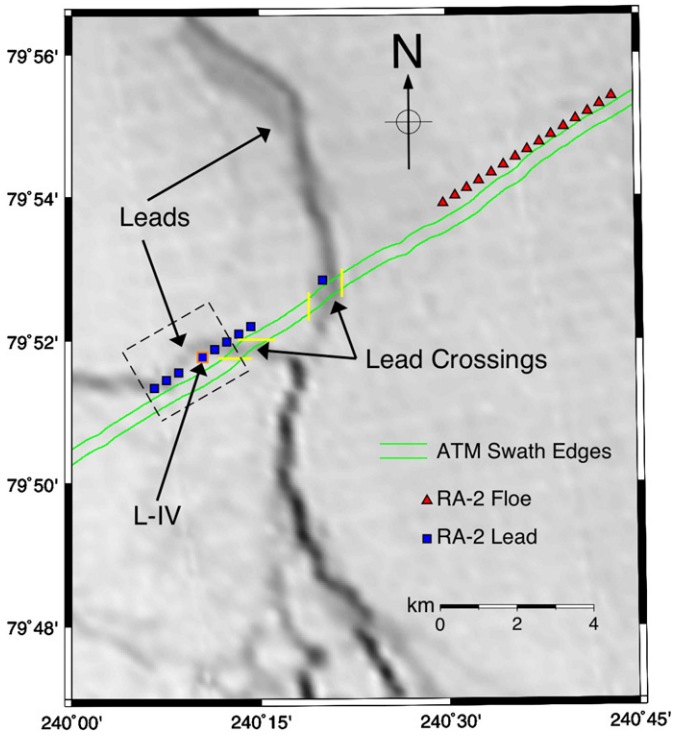

Fig. 5. MODIS 250 m visible imagery over "Lead 2" region at 23:50 UTC on March 27, 2006. Darker lines indicate leads and refrozen leads. Red triangles and blue squares correspond to the footprint center point locations of RA-2 floe and lead elevation estimates, respectively. Green lines show the edges of the ATM swath coverage. Note the lead line in the MODIS image running parallel to, but outside of the ATM swath near the clustered RA-2 lead estimates. Yellow bars indicate leads crossing the ATM swath. The dashed box enclosing the cluster of RA-2 lead locations (blue squares; including L-IV bordered in orange) depicts border of Fig. 6. RA-2 overpass time: 21:45 UTC. ATM underflight time: 21 12 UTC. (For interpretation of the references to colour in this figure legend, the reader is referred to the web version of this article.)

and red triangles corresponding to the RA-2 lead and floe type points, respectively, shown in the Lead 2 profile of Fig. 4. ATM measurements at this location occurred at approximately 21:12 UTC and the RA-2 measurements took place at 21:45 UTC, 2.6 h and 2.1 h before the MODIS pass for ATM and RA-2 measurements, respectively. Thus, even substantial drift velocities in the ice field on the order of 100 m/hr (Emery et al., 1997; Kwok et al., 1998) would produce MODIS image ice field displacements of only 210 m and 260 m relative to the RA-2 and ATM measurements, respectively.

At the location of the first four RA-2 lead points in Fig. 5 (farthest left), a lead may be seen aligned parallel to the ATM swath track, but offset by 500–1000 m to the northwest. Near these RA-2 lead points, the RA-2 footprint will encompass the lead while the ATM will see only floe ice. Fig. 6 demonstrates this scenario for the single RA-2 lead estimate labeled L-IV in Figs. 4 and 5. The RA-2 footprint for L-IV is represented by the 2 km diameter shaded disk along with a section of ATM swath data. The RA-2 measurement picks up a strong lead signal located at a position outside the ATM swath, while the ATM collocated elevation is simply the mean elevation calculated over a 2 km length of ATM swath data centered near the RA-2 lead point location. The RA-2 elevation is then subtracted from the ATM elevation to build the comparison statistics represented in Fig. 4b. However, this now results in an elevation difference that is a floe elevation with snow cover (ATM) minus a lead elevation (RA-2). Thus, the calculated residuals for such points can be larger than the differences found in the floe histogram of Fig. 3a, which are a result of snow cover alone. This is consistent with the Lead 2 profile of Fig. 4 where the ATM spatial means show a local elevation maximum (2000–4000 m along-track), but the RA-2 measures lower lead elevations.

Such measurement configurations can result in misleadingly large differences between ATM and RA-2 elevations and explain the large spread of elevation residuals seen in the lead histogram of Fig. 3b. Further along the ATM track shown in Fig. 5, the lead crosses the ATM swath and a decrease may be seen in the ATM elevations (Lead 2 profile of Fig. 4) as the lead and floe elevations mix in the spatial mean. A couple of kilometers further along the track a large lead crosses the ATM swath producing a strong lead signal in both the ATM and RA-2 processing. Still further along the track both the RA-2 and ATM view only snow covered floe ice. Being completely isolated from the influence of lead specular scattering, this last configuration corresponds to the Floe Type histogram of Fig. 3a, where snow accumulation alone is responsible for the elevation differences.

To address these challenges in evaluating each RA-2 lead classification and lead height estimate, a new analysis was carried out on particular segments of ATM data to identify probable regions of lead type surfaces. At each RA-2 point classified as a lead, the ATM elevations within a 2 km window centered on the particular RA-2 point (and representative of the ATM data within the RA-2 footprint) were again selected. A 200 m sliding sub-window was then propagated along-track through the 2 km section of ATM data in 10 m increments, calculating the mean and standard deviation of the ATM elevations within the smaller sub-window. The resulting 200 m sub-window ATM data set was visually examined surrounding the RA-2 lead points and relative to both the original high-resolution ATM data and the available photo imagery. Using this comparison it was possible to establish lead detection criteria from the 200 m sub-window ATM statistics. To apply these criteria each RA-2 lead point was examined for surrounding (±1 km) 200 m ATM data that met three requirements: 1.) The elevation standard deviation is less than 90 cm, 2.) The elevation mean is at least 40 cm below the maximum mean elevation over the range ±4 km from the RA-2 lead point, 3.) The elevation mean is no more than 6 cm above the minimum mean elevation over the range ±4 km from the RA-2 lead point. The first requirement specifies flatness, providing an absolute maximum threshold for lead elevation variability. The second requirement ensures the local presence of floe ice and, through comparison, that the flat area being examined is not simply an area of flat floe ice. The third requirement is similar to the second in that it verifies that points are local low points. The points meeting these criteria for a given RA-2 lead point are examined and the one with the lowest elevation standard deviation is selected and its associated mean

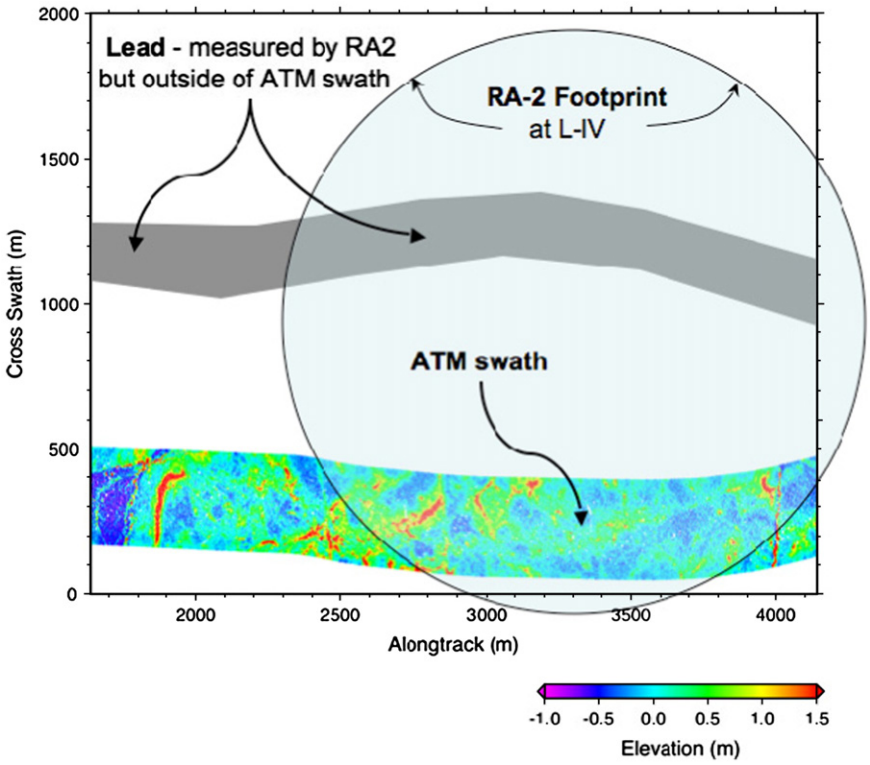

Fig. 6. RA-2 footprint and ATM swath track associated with the L-IV lead point. The ATM swath samples a limited portion of the RA-2 footprint and misses the highly reflective lead surface responsible for the RA-2 elevation estimate. For precise location compare with Fig. 5.

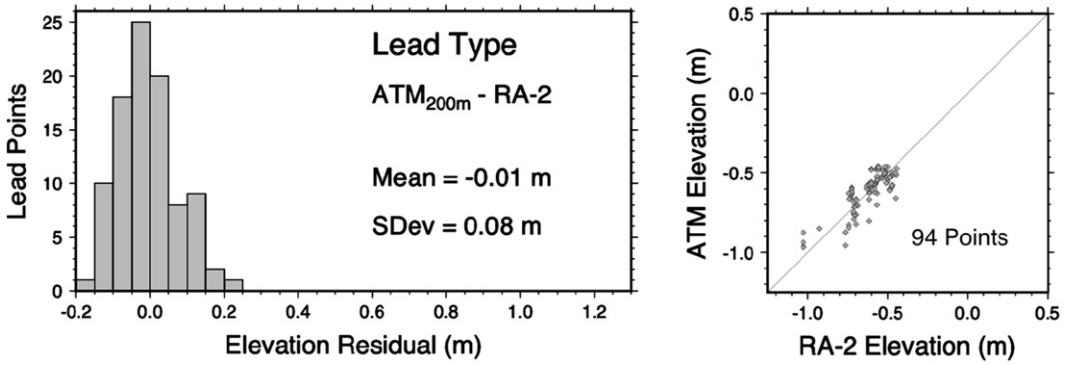

Fig. 7. Histogram representation (left) of the differences of ATM 200 m lead elevations and RA-2 lead type elevations. ATM 200 m lead elevations are determined from ATM lead detection analysis. A scatter plot of the ATM and RA-2 lead type elevations is shown to the right of the floe histogram.

elevation is designated as the ATM lead elevation collocated with the RA-2 lead point.

Fig. 7 shows the resulting lead elevation histogram and scatter plot when the new lead detection analysis is used to determine lead elevations in the ATM swath measurements. The ATM-RA2 elevation residual now shows a dominant primary peak centered near zero (residual mean is −1 cm) and having a width of about ±15 cm (residual standard deviation is 8 cm). This near-zero bias is qualitatively consistent with refrozen leads having very little or no snow cover, particularly when compared to the floe histogram peak location in Fig. 3a and serves to emphasize the impact snow accumulation can have on ATM measurements. The large residual values noted in the previous lead elevation comparison of Fig. 3b have vanished, as expected with the identification and designation of lead surfaces in the ATM swath for comparison. Put simply, the ATM floe ice elevations have been filtered out and RA-2 lead elevations are compared to ATM lead elevations. The scatter plot also demonstrates good agreement between the ATM and RA-2 lead elevation measurements, showing a tight and symmetric clustering of points near the perfect correlation line. Note that the implementation of the new lead detection criteria in analyzing the ATM elevations measurements reduced the number of comparable lead elevation pairs (RA-2 lead type and ATM 200 m means) from 157 to 94, a drop of 40%. This makes detailed statistical analysis of lead elevations difficult and serves to emphasize the spatial sampling problems inherent in validating RA-2 elevations of dynamic sea ice surfaces.

6. Summary

Statistical comparisons between Envisat RA-2 and averaged airborne laser elevation (ATM) measurements along the AAA flight track reveal a good overall consistency between RA-2 and ATM elevations. Our analysis shows that over floe ice, elevation estimates from RA-2 waveform data tend to be lower than corresponding ATM estimates, the average difference being 36 cm. This may be attributed to snow accumulation and is consistent with arctic snow depth climatology. Moreover, this 36 cm disparity over floe ice supports the hypothesis that the laser (ATM) measures snow surface elevation while the radar (RA-2) measures the elevation of the underlying ice/snow interface. Envisat RA-2 sea ice elevation estimates agree closely with ATM measurements over refrozen lead surfaces with negligible snow accumulation, with a mean difference on the order of 1 cm. The ± 10–15 cm spread observed in these differences may result from ocean tide differences, inverse barometer corrections, snow accumulation not discernable from the photo imagery, or issues associated with the ATM's partial and offset sampling of the RA-2 footprint. Careful examination of the ATM and RA-2 sampling geometries and MODIS visible imagery revealed occurrences of lead specular scattering dominating RA-2 elevation estimates over predominantly floe ice. A procedure was developed to detect highly reflective lead surfaces within the ATM swath coverage, resulting in the excellent lead elevation agreement between ATM and RA-2. Elevation comparisons between the two instruments are complicated, however, as some RA-2 measurements originate from lead surfaces outside of the ATM swath. Our analysis indicates that the RA-2 reflections can come from very small lead surfaces (significantly smaller than the nominal 2 km RA-2 footprint). This serves to increase the uncertainty brought on by the spatial offset between RA-2 and ATM ground tracks and to act as a major error source in ATM—RA-2 elevation comparisons.

The analysis difficulties and ambiguities revealed in this study strongly suggest a need for collocated high-resolution measurements of the ice/snow interface elevation. This need may be met by combining, with the ATM data, data collected from the Johns Hopkins University, Applied Physics Laboratory Delay-Doppler Phase Monopulse (D2P) Ku-band Radar Altimeter (Giles et al., 2007; Leuschen & Raney, 2005) that was also operating on the NASA P-3 during the AAA flight. Future work will aim to use D2P, ATM, and in situ measurements to better quantify the impact of snow accumulation on sea ice freeboard retrievals from the RA-2 and will seek to identify elevation bias sources and establish a reliable sea surface height using elevation measurements at open leads. This will enable more precise ice/snow freeboard measurement along the AAA flight path. Data from the D2P will further be used to quantity the impact of refrozen lead surfaces on radar elevation measurements over sea ice. A parallel investigation is also underway using ATM data which were also collected during this same March 27, 2006 AAA campaign to validate ICESat laser altimeter sea ice elevations.

Acknowledgments

The authors wish to thank the NASA P-3 Aircrew for their support during the AAA 2006 Campaign and Serdar Manizade and Chreston Martin for their expertise and assistance with the ATM data processing. The March 27, 2006 AAA flight was supported by NOAA and NASA. The views, opinions, and findings contained in this report are those of the authors and should not be construed as an official National Oceanic and Atmospheric Administration or US Government position, policy, or decision.

References

Bamber, J. L. (1994). Ice sheet altimeter processing scheme. *International Journal of Remote Sensing*, *15*, 925–938.

Beaven, S. G., Lockhart, G. L., Gogineni, S. P., & Hosseinmostafa, A. R. (1995). Laboratory measurements of radar backscatter from bare and snow-covered saline ice sheets. *International Journal of Remote Sensing*, *16*, 851–876.

Carrère, L., & Lyard, F. (2003). Modeling the barotropic response of the global ocean to atmospheric wind and pressure forcing—comparisons with observations. *Geophysical Research Letters*, *vol. 30*(6), 1275. doi:10.1029/2002GL016473

Chelton, B. C., Ries, J. C., Haines, B. J., Fu, L., & Callahan, P. S. (2001). Satellite altimetry. In L. Fu & A. Cazenave (Eds.), *Satellite Altimetry and Earth Sciences: An Handbook of Techniques and Applications* (pp. 1-131): Academic Press.

Comiso, J. C. (2002). Correlation and trend studies of the sea-ice cover and surface temperatures in the Arctic. *Annals of Glaciology*, *34*, 420–428 34.

Drinkwater, M. R. (1991). Ku band airborne radar altimeter observations of marginal sea ice during the 1984 marginal ice zone experiment. *Journal of Geophysical Research*, *96*, 4555–4572.

Emery, W. J., Fowler, C. W., & Maslanik, J. A. (1997). Satellite-derived maps of Arctic and Antarctic sea ice motion: 1988 to 1994. *Geophysical Research Letters*, *24*, 897–900.

ESA (2007). *ENVISAT RA2/MWR Product Handbook*. European Space Agency.

Farrell, S. L. (2007). Satellite laser altimetry over sea ice. *Department of Space and Climate Physics* (pp. 224). London: University College London.

Fetterer, F. M., Drinkwater, K. C., Jezek, K. C., Laxon, S. W. C., Onstott, R. G., & Ulander, L. M. H. (1992). Sea ice altimetry. In F. Carsey (Ed.), *Microwave Remote Sensing of Sea Ice* (pp. 111–135). Washington, D. C.: AGU.

Giles, K. A., Laxon, S. W., Wingham, D. J., Wallis, D. W., Krabill, W. B., Leuschen, C. J., et al. (2007). Combined airborne laser and radar altimeter measurements over the Fram Strait in May 2002. *Remote Sensing of the Environment*, *111*, 13.

Iijima, B. A., Harris, I. L., Ho, C. M., Lindqwister, U. J., Mannucci, A. J., Pi, X., et al. (1999). Automated daily process for global ionospheric total electron content maps and satellite ocean altimeter ionospheric calibration based on Global Positioning System data. *Journal of Atmospheric and Solar-Terrestrial Physics*, *61*(16), 1205–1218.

Krabill, W. B., Abdalati, W., Frederick, E. B., Manizade, S. S., Martin, C. F., Sonntag, J. G., et al. (2002). Aircraft laser altimetry measurement of elevation changes of the Greenland ice sheet: technique and accuracy assessment. *Journal of Geodynamics*, *34*, 357–376.

Kwok, R., Schweiger, A., Rothrock, D. A., Pang, S., & Kottmeier, C. (1998). Sea ice motion from satellite passive microwave imagery assessed with ERS SAR and buoy motions. *Journal of Geophysical Research-Oceans*, *103*, 8191–8214.

Kwok, R., Zwally, H. J., & Yi, D. (2004). ICESat observations of Arctic sea ice: a first look. *Geophysical Research Letters*, *31*, L16401. doi:10.1029/2004GL020309

Laxon, S. (1994). Sea ice altimeter processing scheme at the EODC. *International Journal of Remote Sensing*, *15*, 915–924.

Laxon, S., Peacock, N., & Smith, D. (2003). High interannual variability of sea ice thickness in the Arctic region. *Nature*, *425*, 947–950.

Leuschen, C. J., Swift, R. N., Comiso, J. C., Raney, R. K., Chapman, R. D., Krabill, W. B., et al. (2008). Combination of laser and radar altimeter height measurements to estimate snow depth during the 2004 Antarctic AMSR-E Sea Ice field campaign. *J. Geophys. Res.*, *113*, C04S90. doi:10.1029/2007JC004285

Leuschen, C. J., & Raney, R. K. (2005). Initial results of data collection by the APL D2P Radar Altimeter over land and sea ice. *Johns Hopkins APL Technical Digest*, *26*, 114–122.

McAdoo, D. C., Wagner, C. A., & Laxon, S. N. (2005). Improvements in Arctic Gravity and Geoid from CHAMP and GRACE: an evaluation. In C. Reigber, H. Luhr, P. Schwintzer, & J. Wickert (Eds.), *Earth Observations with CHAMP: Results from Three YEars in Orbit* (pp. 37–46). Berlin: Springer.

McLaren, A. J., Banks, H. T., Durman, C. F., Gregory, J. M., Johns, T. C., Keen, A. B., et al. (2006). Evaluation of the sea ice simulation in a new coupled atmosphere-ocean climate model (HadGEM1). *Journal of Geophysical Research-Oceans*, *111*, C12014. doi:10.1029/2005JC003033

Peacock, N. R., & Laxon, S. W. (2004). Sea surface height determination in the Arctic Ocean from ERS altimetry. *Journal of Geophysical Research-Oceans*, *109*, C07001. doi:10.1029/2001JC001026

Rothrock, D. A., Yu, Y., & Maykut, G. A. (1999). Thinning of the Arctic sea-ice cover. *Geophysical Research Letters*, *26*, 3469–3472.

Tapley, B. D., Ries, J. C., Davis, G. W., Eanes, R. J., Schutz, B. E., Shum, C. K., et al. (1994). Precision orbit determination for Topex/Poseidon. *Journal of Geophysical Research-Oceans*, *99*, 24383–24404.

Warren, S. G., Rigor, I. G., Untersteiner, N., Radionov, V. F., Bryazgin, N. N., Aleksandrov, Y. I., et al. (1999). Snow depth on Arctic sea ice. *Journal of Climate*, *12*, 1814–1829.

Zwally, H. J., Donghui, Y., Kwok, R., & Zhao, Y. (2008). ICESat measurements of sea ice freeboard and estimates of sea ice thickness in the Weddell Sea. *Journal of Geophysical Research*, *113*, C02S15. doi:10.1029/2007/JC004284